

# Electronic and Phonon Instabilities in Bilayer Graphene under Applied External Bias

E. Lora da Silva<sup>1,2</sup>, M. C. Santos<sup>3</sup>, J. M. Skelton<sup>4</sup>, Tao Yang<sup>5,6</sup>,  
T. Santos<sup>7</sup>, S. C. Parker<sup>2</sup>, A. Walsh<sup>8</sup>

<sup>1</sup>Instituto de Diseño para la Fabricación y Producción Automatizada, and MALTA  
Consolider Team, Universitat Politècnica de València, 46022 València, Spain

<sup>2</sup>Department of Chemistry, University of Bath, Bath BA2 7AY, United Kingdom

<sup>3</sup>Department of Physics, University of Coimbra, 3004-516 Coimbra, Portugal

<sup>4</sup>School of Chemistry, University of Manchester, Oxford Road, M13 9PL, United  
Kingdom

<sup>5</sup>Key Laboratory of Biofuels, Qingdao Institute of Bioenergy and Bioprocess  
Technology, Chinese Academy of Sciences, Qingdao, 26610, China

<sup>6</sup>TEMA-NRG, Department of Mechanical Engineering, University of Aveiro,  
3810-193 Aveiro, Portugal

<sup>7</sup>CICECO, Department of Physics, University of Aveiro, 3810-193 Aveiro, Portugal

<sup>8</sup>Department of Materials, Imperial College London, London SW7 2AZ, United  
Kingdom

E-mail: e1ds22@bath.ac.uk

September 2018

**Abstract.** We have performed electronic-structure and lattice-dynamics calculations on the AB and AA structures of bilayer graphene. We study the effect of external electric fields and compare results obtained with different levels of theory to existing theoretical and experimental results. Application of an external field to the AB bilayer alters the electronic spectrum, with the bands changing under bias from a parabolic to a "Mexican hat" structure. This results in a semi-metal-to-semiconductor phase transition, with the size of the induced electronic band-gap being tuneable through the field strength. A reduction of continuous symmetry from a hexagonal to a triangular lattice is also evidenced through in-plane electronic charge inhomogeneities between the sublattices. When spin-orbit coupling is turned on for the AB system, we find that the bulk gap decreases, gradually increasing for larger intensities of the bias. Under large bias the energy dispersion recovers the Mexican hat structure, since the energy interaction between the layers balances the coupling interaction. We find that external bias perturbs the harmonic phonon spectra and leads to anomalous behaviour of the out-of-plane flexural ZA and layer-breathing ZO' modes. For the AA system, the electronic and phonon dispersions both remain stable under bias, but the phonon spectrum exhibits zone-center imaginary modes due to layer-sliding dynamical instabilities.

*Keywords:* Bilayer graphene, electric field, electronic properties, lattice dynamics

## 1. Introduction

Among the numerous derivatives of the monolayer graphene (MLG) system, special interest has been given to the multi-layer allotropes [1], in particular *Bernal* bilayer graphene with AB stacking (AB-BLG) [2]. Like ML graphene, BL graphene also displays unconventional properties [3] that are relevant to technological developments including tunnelling field-effect transistors [4], high-rate lithium-sulphur batteries [5, 6], nanophotonics [7], sensor modelling [8], among others. These properties originate from the weak coupling between layers, which allows for the properties of the base ML graphene material to be retained. Despite the similarities between ML and BL graphene, there are also significant differences between the two allotropes. ML graphene shows a linear band dispersion near the Fermi energy, and the valence and conduction bands touch at the  $K$ -point (the Dirac point), yielding the characteristic dispersion of relativistic massless Dirac electrons [9, 10]. For unbiased AB-BLG, on the other hand, the interlayer coupling produces a parabolic-like band structure around the  $K$ -point. These different features result in a vanishing of the density-of-states (DOS) at the Fermi energy for the MLG [10], in contrast to a finite DOS evidenced in the AB-BLG.

Another characteristic feature of AB-BLG is the behaviour of the system when an electric field is applied normal to the layers. It has recently been shown that biased AB-BLG can form a Wigner crystal, due to the existence of different kinetic-energy dispersions at different electron densities [11]. The energy band gap can be tuned in proportion to the intensity of the applied bias [2], and two distinct zero-temperature quantum phases at different electron densities can be formed [11, 12].

For the AB-BLG system, the presence of significant SOC has been evidenced by topological-insulator behaviour with a finite spin Hall conductivity [13]. Moreover, it has also been shown that biased BLG may exhibit two topologically-distinct phases depending on the intensity of the Rashba spin-orbit coupling (RSOC) [14]. For weak coupling, the system exhibits a quantum-valley Hall state, which can then transition to a topological insulator in the presence of strong coupling effects. It is possible to transition between these two phases by tuning the applied electric field [14]. In the presence of strong RSOC, and for sufficiently short-range electron-electron interactions, the system minimises its energy by adopting broken-symmetry states (mostly those which break rotational symmetry) in the limit of low densities [15]. These instabilities occur due to the energy dispersion having a minimum in a region of momentum-space which is bounded by two concentric circles with finite radius (annuli) [16]. Moreover, distortions to the Fermi surface, resulting from a momentum-space change in the Fermi radius (a Pomeranchuk instability) can reduce the lattice symmetry and lead to spontaneous longitudinal currents [16].

Another stacking arrangement of BL graphene, which coexists with the AB stacking, is the AA structure where the carbon atoms are positioned directly above each other in consecutive layers. The electronic properties differ from those of AB-BLG due to the the stacking arrangement. AA stacking has been experimentally observed

in disordered or pregraphitic carbon, also known as turbostratic graphite, and can be distinguished from ML graphene by so-called tilting experiments [17, 18]. However, as the space groups of AA-BLG and MLG are the same ( $P6/mmm$ ), similarities between the two are difficult to predict.

Between the two stacking environments, the AB stacking is the most energetically-favourable form, and is separated from the AA stacking by a small energy barrier. Despite its instability, AA-BLG has started to receive significant attention. The AA configuration shows unusual electronic properties, with two degenerate electronic and hole bands crossing at the Fermi energy [19]. This electronic structure supports several electron and electron-phonon instabilities, which include, among others, a shear-shift instability [19]. It has further been observed that small perturbations can destabilize the degenerate spectrum and generate an excitonic gap [19, 20]. .

While the AB-BLG system is well studied both experimentally and theoretically, comparatively less attention has been given to the AA stacking. In the present work, we aim to provide more insight into the electronic and vibrational properties of biased AA-BLG, and to make a comparison to the AB-system, by employing first-principles simulation techniques.

We find that while the AB system presents variations on the electronic densities as a function of the applied bias, we observe that the AA system remains unaltered when an electric field is applied. SOC effects are also considerable for the biased AB-system, with the band-gap presenting different scaling behaviours according to the field intensities. The phonon dispersions of the biased AB system shows instabilities of the out-of-plane acoustic and optic modes, when compared to the stability of these modes for the unbiased system. On the other hand, phonon dispersions of the AA system remain stable under bias, but the phonon spectrum exhibits a zone-center imaginary mode resulting from the shear-mode instability.

## **2. Theoretical Framework**

We study the electronic structure of the two different stacking environments of the BLG system (crystal structure of AB- and AA-BLG presented in figure 1) using density-functional theory (DFT) with the Local-Density Approximation (LDA) functional. An external electric field is applied in the direction of the interlayer plane with variable magnitude. Lattice dynamics are performed within the harmonic approximation, which yields phonon frequencies and the constant-volume terms in the free energy from lattice vibrations.

### *2.1. Density Functional Theory*

Electronic-structure calculations were performed within the pseudopotential plane-wave density-functional theory (DFT) framework, as implemented in the *Vienna Ab-initio Simulation Package* (VASP) [21, 22, 23] code. The Ceperley and Alder form of the

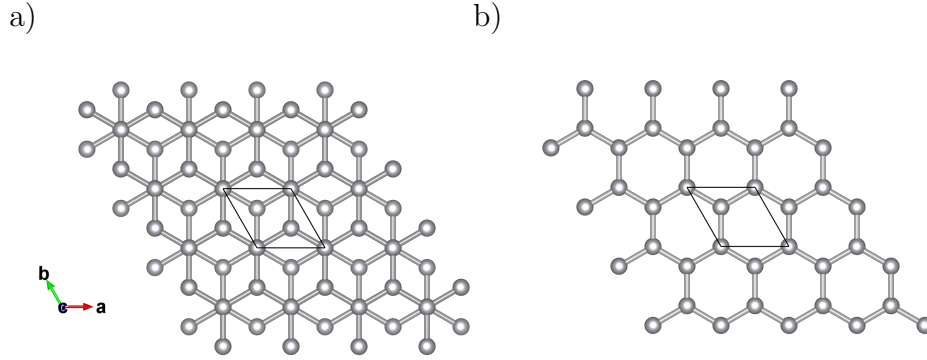


**Figure 1.** Supercell of the AB- (space group  $P - 3m1$ ,  $n^\circ$  164; a) and AA-BLG (space group  $P6/mmm$ ,  $n^\circ$  191; b) systems, where the black line shows the unit-cell. BLG consists of two coupled monolayers of carbon atoms, each with a honeycomb crystal structure. In order to satisfy the translational and symmetry properties of the Bravais lattice, the honeycomb lattice can be seen as two triangular sublattices, mathematically labelled as inequivalent  $A$  and  $B$  lattices, each of which contains two atoms in the unit cell within each  $C$  sheet, with atom  $[a_1, a_2] \in A$  and  $[b_1, b_2] \in B$  for layer 1 and 2. The layers of the AB-BLG are arranged in such a way that one of the atoms from the lower-layer  $b_1$  is directly below atom  $a_2$  from the upper layer, and the remaining two atoms,  $a_1$  and  $b_2$ , are shifted from each other by a vector displacement [10]. For the AA-BLG, the carbon atoms are aligned in the consecutive layers, directly above/below each other ( $a_1$  with  $a_2$  and  $b_1$  with  $b_2$ ).

Local-Density Approximation (LDA) functional, parametrised by Perdew and Zunger [24], was used in conjunction with projector augmented-wave (PAW) pseudopotentials [25, 26]. We selected the LDA functional because it is known to perform well at capturing the interlayer distance in graphite and multi-layer graphene allotropes, as well as the essential physics of the electronic structure, and also performs well for calculating interatomic force constants and phonon frequencies [27, 28].

A plane-wave cut-off of 800 eV was applied in all calculations; although convergence of the electronic structure was attained at a lower cut-off of  $\sim 600$  eV, a higher value was chosen to improve the description of the structural parameters and forces, which is important for accurate lattice-dynamics calculations [29]. The Brillouin zone (BZ) was sampled with  $\Gamma$ -centred Monkhorst-Pack meshes [30] with  $44 \times 44 \times 1$  and  $90 \times 90 \times 1$  subdivisions for AA- and AB-BLG respectively. It was found necessary to employ the denser  $\mathbf{k}$ -point mesh for the AA-BLG model due to differences in the DFT electronic band structure relative to the spectra expected from tight-binding theory (section Appendix A). The vacuum spacing between periodic images along the  $Z$  direction was set to 15 Å for both configurations, and dipole corrections to the potential were applied to avoid interactions between periodic images.

Lattice-dynamics calculations were carried out using the Parlinski-Li-Kawazoe supercell finite-displacement method [31, 32], which is implemented in the Phonopy [33, 34] package; a detailed description of the theoretical implementation can be found in Refs. [35, 29]). The interatomic force constants were obtained by performing single-point

force calculations on a series of symmetry-inequivalent displaced structures and fitting the resulting force/displacement curves to a harmonic function. VASP was used as the force calculator [32] and the calculations were performed on  $4 \times 4 \times 1$  supercells using a reduced  $\mathbf{k}$ -point sampling mesh of  $12 \times 12 \times 1$  for both phases. For the calculations under bias, the electric field was applied during the force-constant calculations. To construct the phonon density of states, the phonon frequencies were sampled on an interpolated  $48 \times 48 \times 1$   $\mathbf{q}$ -point mesh.

A non-analytical correction (NAC) was applied when computing the phonon-band dispersion [36] to correct for long-range Coulomb interactions. The requisite Born effective-charges and static dielectric constant were computed using the density-functional perturbation theory (DFPT) routines implemented in VASP [37]. Convergence of these quantities required increasing the  $\mathbf{k}$ -point mesh for the AB system up to  $80 \times 80 \times 1$ , whereas for the AA system the  $90 \times 90 \times 1$  mesh was found to be sufficient.

A bias was applied in the calculations as an external electrostatic field in the  $Z$  direction and geometries were re-optimised with different intensities of the field. Born effective-charges and dielectric tensors were calculated by considering the field perturbations. For the lattice-dynamics calculations, the bias was also applied during the calculations of the force constants.

### 3. Results and Discussion

The lattice parameters obtained within the LDA are  $a_0=2.42 \text{ \AA}$  and  $c_0=6.69 \text{ \AA}$  for the AB system, and  $a_0=2.45 \text{ \AA}$  and  $c_0=6.67 \text{ \AA}$  for the AA system. The intra-layer distance (C-C bond lengths) are on the order of  $1.41 \text{ \AA}$  in both stacking environments, and the interlayer distance was calculated to be  $3.35 \text{ \AA}$  and  $3.34 \text{ \AA}$  for the AB and AA configurations, respectively. The parameters for AB-BLG are in agreement with those discussed in Ref. [38], where the calculations were also performed with DFT-LDA (intra-layer distance of  $1.41 \text{ \AA}$  and interlayer distance of  $3.31 \text{ \AA}$ ). The present interlayer parameters also compare well to experimental results, where for the Bernal graphite the value of  $3.35 \text{ \AA}$  [39] was observed. However, for the AA-BLG the present interlayer distance is found to be slightly lower than results found in literature:  $3.59 \text{ \AA}$  from DFT-LDA calculations [38], and  $3.55 \text{ \AA}$  from experimental observations on the AA graphite structure [40].

#### 3.1. Electronic Spectrum from a Density-Functional and Tight-Binding Perspective

To study the electronic structure, we calculated the low-energy band dispersions using LDA-DFT with three intensities of applied electric field. The results are presented in figure 2. For the AB-BLG configuration (Figure 2.a), when  $E = 0 \text{ eV/\AA}$ , a zero-gap parabolic dispersion around the  $K$ -point is observed. The LDA-DFT electronic dispersion for the AB system shows similar features to the band-structure obtained

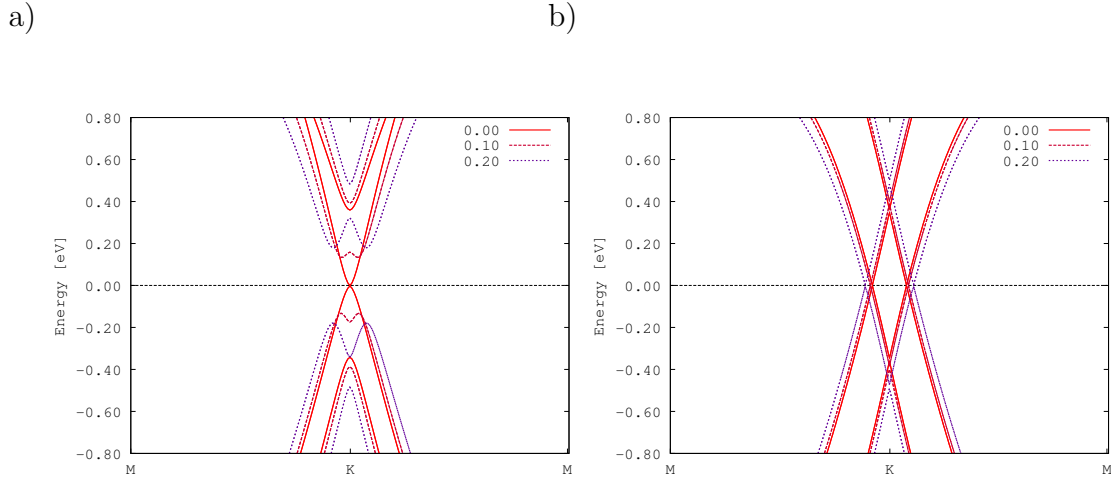


**Figure 2.** Low-energy DFT-LDA electronic band-structure of bilayer graphene with AB (a) and AA (b) stacking arrangements. Each dispersion is shown at different applied field intensities (label units given in  $\text{eV}/\text{\AA}$ ).

from the tight-binding Hamiltonian (figure A1, Appendix A).

When a finite electric-field is applied perpendicular to the graphene layers in AB-BLG, the two layers are subject to inequivalent potentials. This effect breaks the inversion symmetry, resulting in the opening of a single-electron gap [2] at the  $K$ -point, which can be tuned up to mid-infrared energies ( $\sim 300$  meV) [41]. A spontaneous translation symmetry breaking also occurs, resulting in a charge separation between the inequivalent sublattices with spatial in-plane charge inhomogeneities [42, 11].

Figure 3 plots the electron charge densities of AB-BLG in the vicinity of the Fermi energy, inspection of which reveals differences between the isosurfaces without (a) and with (b) a bias applied. In the unbiased system (figure 3.a), the charge densities show hexagonal symmetry, indicating homogeneous electron delocalisation between the sublattices. On the other hand, when an interlayer electric field is applied (figure 3.b), redistribution of electron densities leads to charge separation between the A and B sublattices, leading to in-plane charge inhomogeneities [11].

The AA-stacking environment differs from the Bernal system by having a linear dispersion with two bands crossing each other at the Fermi energy [10]. Application of an external field does not alter the width of the band gap, and electronic structure remains qualitatively the same. This single-electron property seems to be quite stable to external bias both in the LDA calculations and also with a tight-binding Hamiltonian [10].

These results are consistent with the electronic dispersion calculated with the tight-binding method (figure A1), although, as noted above, obtaining a fully-converged dispersion from the DFT calculations required very dense  $\mathbf{k}$ -point sampling. This is because the band crossing does not occur at a high-symmetry  $\mathbf{k}$ -point, and thus a dense

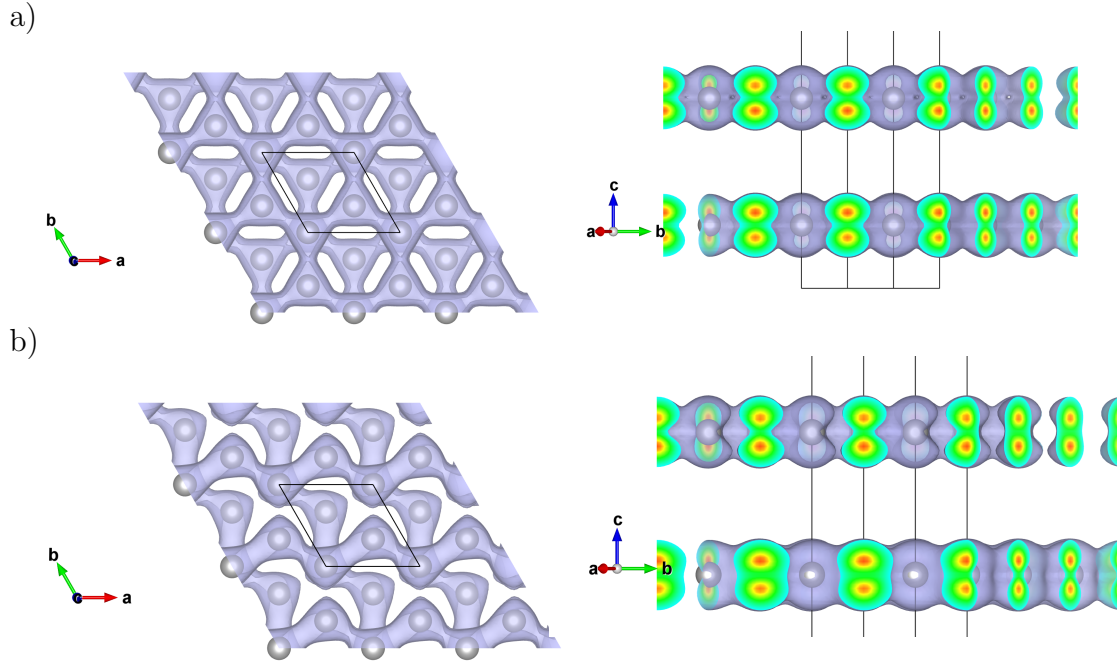


**Figure 3.** Two different views (top and side) of the isosurfaces (value defined at 0.016) of the electron charge densities around the Fermi energy for the AB-BLG system without (a) and with (b) an applied bias (electric field intensity of 0.05 eV/Å).

mesh is required in order to include sufficient sampling around the feature to accurately represent the bands in the vicinity of the Fermi energy.

Under bias, the dispersion relations of the AB system show a "Mexican hat" structure [2, 43]. With increasing field intensity, the width of the gap increases and the radius of the hat feature widens, with the two minima getting progressively further apart from the  $K$ -point [2]. This behaviour is consistent with the results from Ref. [11], which suggest that regions of the dispersion should exhibit different scaling behaviour as a function of momentum [11]. Moreover, controlling the magnitude of the gap through additional screening with a transverse electric field will afford control over the density of electrons [44].

Figure 4.a shows the electronic band-structure when spin-orbit coupling (SOC) is included in the calculations.

In the present study, we find that the bulk gap decreases when SOC is turned on, and then increases gradually for increasing field intensities (Figure 4.a) Under large field intensities ( $\sim 0.4$  eV/Å), the energy dispersion recovers the Mexican hat structure, since the instability occurring at the Fermi-surface competes with the SOC interaction; the energy interaction between the layers balances the coupling interaction.

Moreover, Ref. [14] reported that the gap vanished as the SOC parameter increases, and that on further increasing the coupling parameter it then reopens with a behaviour characteristic of a band inversion, thus suggesting a topological phase transition [14]. However, since the model employed in [14] is different from the computations carried

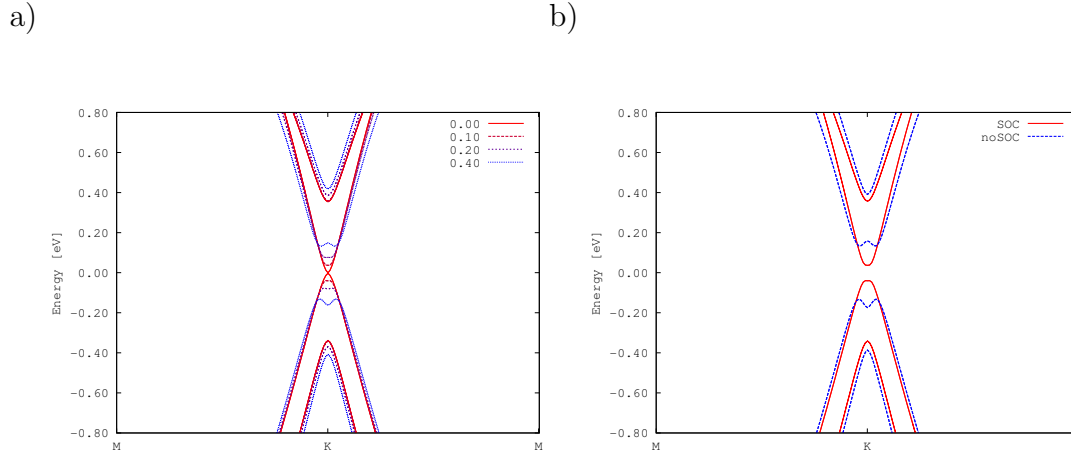


**Figure 4.** Low-energy DFT-LDA electronic band-structure of AB-stacked bilayer graphene. (a) Dispersions with different intensities of an applied external interlayer electric field, calculated with spin-orbit coupling. (b) Dispersions of a biased system ( $E = 0.20 \text{ eV/\AA}$ ) with and without spin-orbit coupling included. Field strengths are given in  $\text{eV/\AA}$ .

out for the presented work, a direct comparison between the two sets of results is not straightforward.

### 3.2. Structural Instabilities of Bilayer Graphene - Lattice-Dynamics

Figure 5 shows the constant-volume (Helmoltz) free energy of the AB and AA bilayer systems calculated without an applied bias. The energies are referenced to the lowest energy structure, which in the present calculations is the AB system. Our calculations indicate that the AA system is energetically unstable with respect to the AB phase up to approx. 800 K, above which the AA stacking becomes lower in energy.

The calculated in-plane phonon dispersion agrees well with the experimental measurements on graphite presented in [45] (Figure 6), apart from a small shift of the higher-frequency TO and LO modes. LDA calculations frequently overestimate the energies of higher-frequency phonons, but despite this difference the characteristic features of the phonon dispersion are well reproduced.

At low  $\mathbf{q}$ -vectors, the in-plane transverse acoustic (TA) and longitudinal acoustic (LA) modes show linear dispersions. Moreover, while the doubly-degenerate LA mode has zero frequency at the  $\Gamma$ -point, the TA mode (also known as the shear-mode) has a non-zero frequency at the zone-center [46] ( $\nu = 0.82 \text{ THz}$ ) (Figure 7).

The ZA mode is the flexural acoustic mode, which corresponds to out-of-plane, in-phase atomic displacements. In contrast to the TA and LA modes, the ZA branch shows a parabolic dispersion, i.e.  $\nu \sim \mathbf{q}^2$ , close to the  $\Gamma$ -point, indicating a low group velocity [47] and being a characteristic feature of layered materials [46, 47]. The existence of a flexural mode is also a signature of 2D systems, and in particular is a mode which



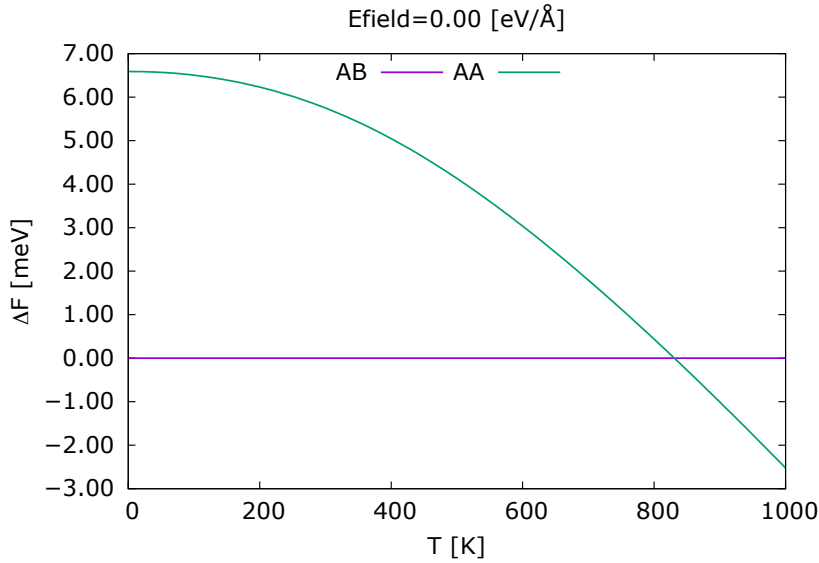


**Figure 5.** Relative free energy (Helmoltz) of the two graphene stacking environments, AB and AA, with no external electric-bias. The AB arrangement is calculated to be the most energetically-stable structure up to  $\sim 800$  K.

is typically found in graphene-like systems. Since the long-wave flexural mode has the lowest frequency, it is the easiest to excite [48].

At slightly higher frequencies, the out-of-plane ZO' mode (Figure 7) can be observed, which corresponds to interlayer motion along the  $Z$ -axis (a layer-breathing mode). The other out-of-plane optic modes are characterised by the doubly degenerate ZO branch. At the  $\Gamma$  point, the interlayer coupling causes the LO and TO modes to split into two doubly-degenerate branches, both of which correspond to in-plane relative motion of atoms. With the exception of the ZA and ZO' modes, all the frequency branches have symmetry-imposed degeneracy at  $\Gamma$  (Figure 6).

Figure 8 compares the phonon dispersions of the two stacking modes. Both stacking configurations have similar mode characters, although differences emerge at the zone-centre.

For the AA system, a small phonon instability is observed at the  $\Gamma$ -point, which is denoted by an imaginary mode ( $\nu = i1.04$  THz). This indicates that the AA-system is dynamically unstable, and prefers to adopt the AB-stacking configuration, in accordance with the free energies in Figure 5. As expected, the imaginary mode is a TA branch, which corresponds to the shear displacement of the layers with respect to one another. The ZA mode also shows instabilities in the vicinity of the zone-center, but has zero frequency at  $\Gamma$ .

The ZO' breathing mode of AA-stacked bilayer graphene is located in a similar frequency range to the corresponding mode in AB graphene, at  $\nu = 2.16$  and  $\nu = 2.25$

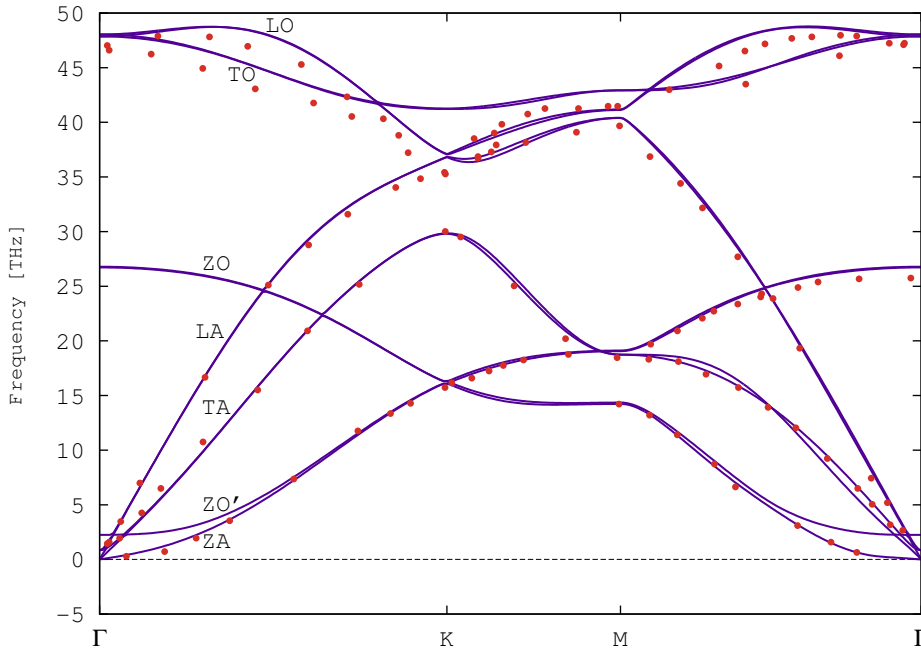


**Figure 6.** Phonon dispersion of AB-stacked bilayer graphene computed within the harmonic approximation (solid line). The unit cell contains four carbon atoms, leading to three acoustic (A) and  $3N - 3 = 9$  optical (O) phonon branches. The calculated dispersions are compared to the in-plane phonon dispersion of graphite obtained from inelastic x-ray scattering [45] (red dots). The phonon branches are marked with the labels assigned to the  $\Gamma$ -point phonons.

THz, respectively. The biggest frequency differences are observed for the TO modes, which in the AB system occurs at higher frequency than in the AA configuration, with 0.72 THz of difference. This is partly because the LO/TO is larger in the AA than the AB system (0.57 and 0.18 THz, respectively).

Table 1 presents a summary of the zone-centre frequencies for the two stacking configurations.

We note that the AA phonon dispersion does not correspond to that in [49], where, in contrast to the present results, imaginary frequencies are not observed (with calculations carried out using the Born-von-Karman model of lattice dynamics for in-plane atomic coupling and the Lennard-Jones potential for interlayer coupling [49]).

The branches which originate from the out-of-plane modes at the  $\Gamma$ -point, i.e. ZA, ZO' and ZO, become degenerate at the K-point (Figure 8)). The in-plane LO and LA phonon branches also meet at the K-point, giving rise to a doubly-degenerate phonon band. It is also noteworthy that the dispersions of the out-of-plane modes behave linearly around the K-point in AA-BLG, whereas those in AB-BLG show a parabolic-

ZA

ZO'

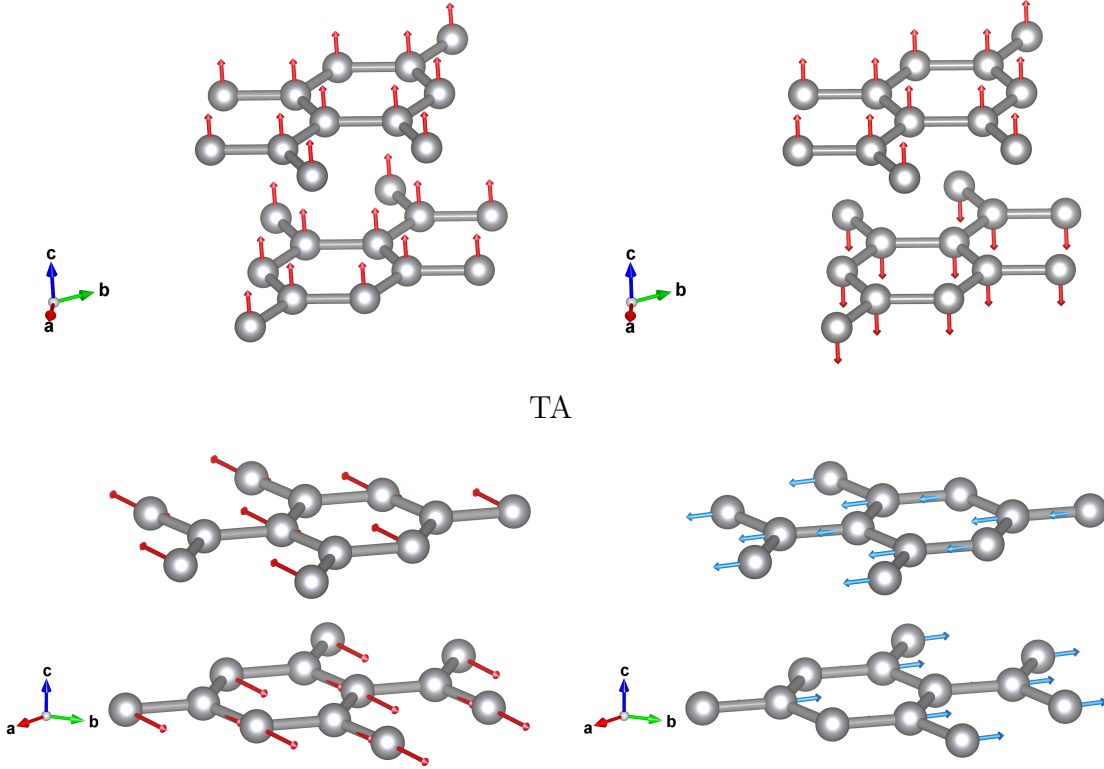


**Figure 7.** Eigenvectors corresponding to the vibrations in AB-stacked bilayer graphene. ZA and ZO' correspond to the out-of-plane vibrations, while TA denotes the degenerate in-plane transverse-acoustic modes.

**Table 1.** Frequencies (THz) of the  $\Gamma$ -point phonon modes in AB- and AA-stacked bilayer graphene.

Mode	ZA	ZO'	TA	LA	ZO	TO	LO
AB	0.00	2.25	0.82	0.00	26.72	47.86	48.04
AA	0.00	2.16	1.04	0.00	26.82	47.14	47.71

like dispersion similar to that suggested in [49]. Features in the electronic spectra near the K-point in the two BLG systems are therefore also reflected in the phonon spectra (c.f. Figures 2 and 8).

Further lattice-dynamics calculations were carried out to investigate the effect of electric fields on the phonon dispersions (Figure 9). Non-analytical corrections to the dynamical matrix at  $q \rightarrow 0$  were considered in all calculations. We find that the dispersion of the AA system is relatively insensitive to the applied external bias, and that for all applied fields the  $\Gamma$ -point instability persists.

In comparison, the low-frequency branches of the AB band-structure show a significant response to the field (Figure 9.a). This effect results from the inclusion of non-analytical corrections; when these corrections are not included, the dispersions

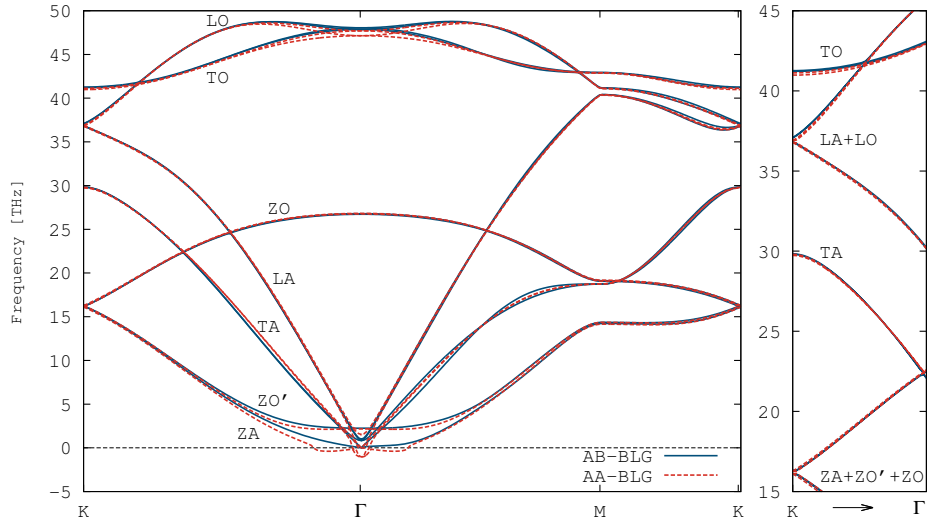


**Figure 8.** Phonon dispersions of the AB- and AA-stacked bilayer graphene systems computed with the harmonic approximation (blue solid and red dashed lines, respectively). The right-hand panel shows the dispersion along the K- $\Gamma$  path. The phonon branches are denoted by the symbols of the  $\Gamma$ -point phonons, several of which become degenerate at the K-point.

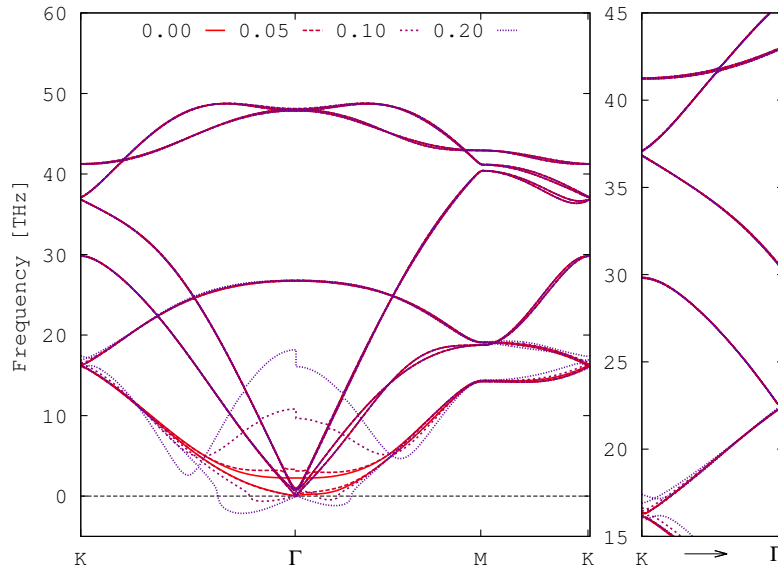
are relatively unaffected by the bias. The layer-breathing mode (ZO') displays a discontinuity at the  $\Gamma$ -point, with different frequencies for different directions of approach. Moreover, the flexural-acoustic (ZA) mode shows instabilities in the vicinity of the zone-centre, but continue to show zero frequency at the  $\Gamma$ -point. Since the long-wave flexural mode has the lowest frequency, it is the easiest to excite [48] and is therefore more sensitive to the bias. At the K-point (Figure 9, inset), as occurs for the electronic band-structure the degeneracy of the out-of-plane modes split, with the magnitude of the splitting depending on the size of the applied bias.

#### 4. Conclusions

In summary, we have performed a detailed first-principles study of the effect of applied fields on the electronic structure and lattice dynamics of bilayer graphene.

Application of an external field to the AB-stacked bilayer graphene system leads to drastic changes in the electronic properties, leading to the opening of the gap and asymmetry in the dispersion. This in turn induces in-plane inhomogeneities in the charge distribution on the sublattices, and the Coulomb interaction between electrons will thus cause a potential difference between the layers. Our results therefore show that the electron density can be controlled by tuning the band-gap width and dispersion asymmetry.

a)



b)

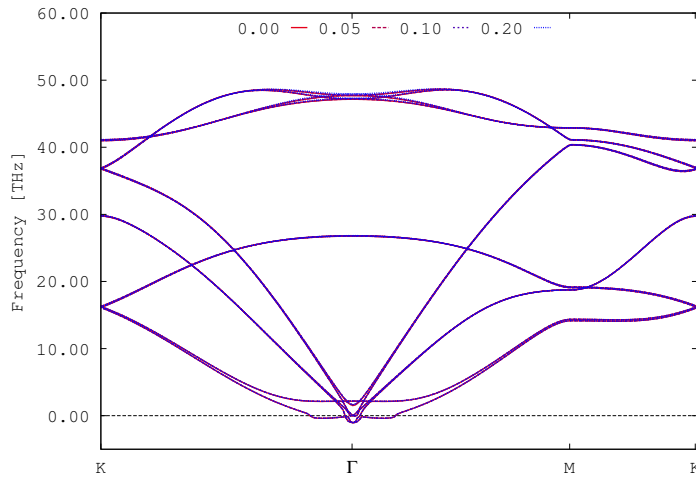


**Figure 9.** Harmonic phonon dispersions of the AB- (a) and AA-stacking (b) configurations of bilayer graphene under different applied bias. The right-hand panel in (a) shows the dispersion along the K- $\Gamma$  segment. The AA system shows doubly-degenerate imaginary modes at the zone-center, which is consistent with the alternative AB stacking being the most favourable arrangement. Non-analytical corrections have been applied to the dispersions of both systems. The ZA and ZO' modes on the AB-BLG change significantly under bias, whereas the applied field has comparatively little effect on the dispersion of the AA-BLG system. Electric fields are given in eV/Å.

Spin-orbit coupling has a significant effect on the dispersion as short-range electron-electron correlations become important. The Mexican-hat structure disappears under low bias, and the energy gap decreases. At larger field strength, the asymmetry in the dispersion persists, since the energy scale set by the Fermi-surface instability is minimized.

On the other hand, the electronic structure of the AA system is relatively stable under bias.

As for its electronic structure, applied fields cause the phonon dispersions of the AB-stacked system to change significantly when non-analytical corrections for long-range Coulomb interactions are taken into account. These corrections mainly affect the lower-frequency out-of-plane ZA and ZO' modes. The phonon dispersion of the AA system shows degenerate imaginary modes at the  $\Gamma$  point, indicating the presence of a phonon instability. The dispersion of this stacking configuration is relatively insensitive to bias and does not change significantly in response to an applied field.

In order to obtain better consistency with available literature, we would need to go beyond LDA functional. The ground-state is likely to have additional broken-symmetry configurations, and the lifting of spin and valley degeneracies may depend on long-range fluctuations, effects which are not well captured by local DFT functionals. For example, in the literature it has been observed that the AA stacking configuration may be stabilised by an excitonic gap [19]. To study such effects, one would need to resort to the two-body Green function method (Bethe-Salpeter equation), a possibility which we are currently exploring.

## **Acknowledgments**

This work was supported by EPSRC Programme Grants (nos. EP/K004956/1 and EP/K016288/1) and the ERC (Grant No. 277757). We acknowledge use of the ARCHER supercomputer through the PRACE Research Infrastructure (award no. 13DECI0313). The authors also acknowledge computing support from the University of Bath Computing Services, which maintains the Balena HPC cluster.

## Appendix A. Tight-Binding Hamiltonian

To study the effects of an applied electric field on bilayer graphene, we begin by describing pure bilayer graphene system with Bernal stacking, considering only the  $t_z$  interlayer hopping amplitude, restricted to the nearest-neighbour carbon atoms. An electric bias  $V = eEd$  is applied in the direction perpendicular to the layers, where  $e$  is the electron charge,  $E$  the applied electric field, and  $d$  the interlayer spacing [2]. The Fermi operators, written as:

$$a_{\mathbf{k}j} = N^{-1} \sum_n e^{i\mathbf{k}\cdot\mathbf{n}} a_{\mathbf{n}j} \quad b_{\mathbf{k}j} = N^{-1} \sum_n e^{i\mathbf{k}\cdot\mathbf{n}} b_{\mathbf{n}j} \quad (\text{A.1})$$

represent plane-wave states with momentum  $\mathbf{k}$ . The indices  $j$  refer to the layers in the  $n$ th unit-cell,  $a_{\mathbf{n}j}$  and  $b_{\mathbf{n}j}$  are operators referring to A- and B-type sites in the lattice (figure 1), and  $N$  is the number of cells in a layer. A 4-spinor is formed by:

$$\psi_{\mathbf{k}}^\dagger = \left( a_{\mathbf{k}1}^\dagger, b_{\mathbf{k}1}^\dagger, a_{\mathbf{k}2}^\dagger, b_{\mathbf{k}2}^\dagger \right). \quad (\text{A.2})$$

The Hamiltonian is given in the second-quantized form by:

$$H_0 = \sum_{\mathbf{k}} \psi_{\mathbf{k}}^\dagger \hat{H}_{\mathbf{k}} \psi_{\mathbf{k}} \quad (\text{A.3})$$

where the matrix has the form:

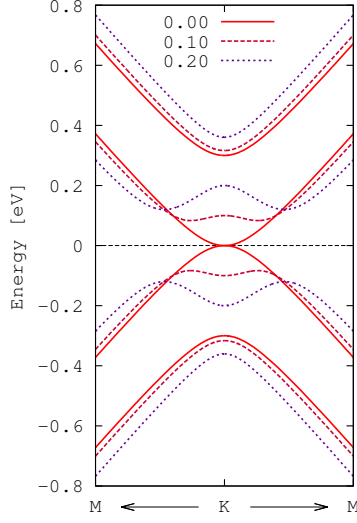
$$\hat{H}_{\mathbf{k}} = \begin{pmatrix} \frac{V}{2} & \gamma_{\mathbf{k}} & 0 & t_z \\ \gamma_{\mathbf{k}}^\dagger & \frac{V}{2} & 0 & 0 \\ 0 & 0 & -\frac{V}{2} & \gamma_{\mathbf{k}} \\ t_z & 0 & \gamma_{\mathbf{k}}^\dagger & -\frac{V}{2} \end{pmatrix} \quad (\text{A.4})$$

The term  $\gamma_{\mathbf{k}} = t \sum_{\boldsymbol{\delta}} e^{i\mathbf{k}\cdot\boldsymbol{\delta}}$  is related to the in-plane hopping amplitude,  $t$ , over the nearest-neighbour vectors  $\boldsymbol{\delta}$  and defined as  $t \approx 3$  according to experimental and first principles calculations suggested in Refs. [50] and [51]). The variable  $\xi_{\mathbf{k}}$  is defined as  $\hbar v_F(\mathbf{k} - K)$ , with the Fermi velocity defined as  $v_F = 3ta/2\hbar \approx 10^{-6}\text{ms}^{-1}$ , and  $a$  being the intra-layer distance between next-neighbour atoms of different sublattices and  $\hbar$  the Planck constant [2]. The interlayer hopping amplitude,  $t_z$ , is related to  $t$  by the relation  $t_z = t/10$  [50].

In the vicinity of the Dirac points  $\pm K$  is defined by  $\pm(4\pi/3\sqrt{3}a, 0)$  and  $\gamma_{\mathbf{k}} \approx \xi_{\mathbf{k}} e^{i\varphi_{\mathbf{k}}}$ , with  $\varphi_{\mathbf{k}} = \tan^{-1} k_y/(k_x - K_x)$  [2]. After diagonalizing the matrix in Eq. A.4, and considering that the dispersion in the vicinity of the Dirac point is defined along a circle around each Dirac point,  $\xi_{\mathbf{k}} \equiv \xi$ , with maximum radius defined as  $\hbar v_F \sqrt{K/a}$  [2], we obtain for the four bands:

$$\begin{aligned} \varepsilon_1(\xi) &= \pm \frac{1}{2} \sqrt{2t_z^2 + V^2 + 4\xi^2 + 2\sqrt{t_z^4 + 4(t_z^2 + V^2)\xi^2}} \\ \varepsilon_2(\xi) &= \pm \frac{1}{2} \sqrt{2t_z^2 + V^2 + 4\xi^2 - 2\sqrt{t_z^4 + 4(t_z^2 + V^2)\xi^2}} \end{aligned} \quad (\text{A.5})$$

a)



b)

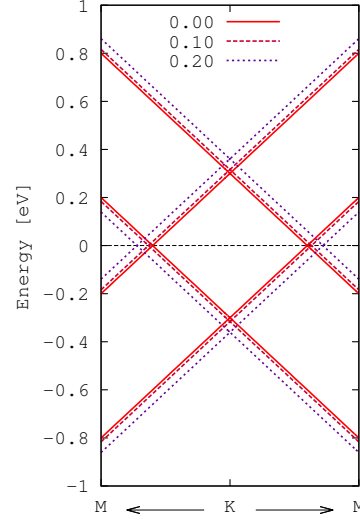


**Figure A1.** Low-energy tight-binding electronic band-structure of bilayer graphene in the AB (a) and AA (b) stacking arrangements. Dispersions are calculated for different intensities of  $V$ .

where  $\varepsilon_1$  and  $\varepsilon_2$  refer to the external and internal bands, respectively [2].

The bias-controlled gap will therefore result in:

$$\varepsilon_g = \pm \frac{V}{2\sqrt{1 + (\frac{V}{t_z})^2}}. \quad (\text{A.6})$$

For the AA-BLG, the calculations are similar, although the matrix takes the form:

$$\hat{H}_{\mathbf{k}} = \begin{pmatrix} \frac{V}{2} & \gamma_{\mathbf{k}} & t_z & 0 \\ \gamma_{\mathbf{k}}^\dagger & \frac{V}{2} & 0 & t_z \\ t_z & 0 & -\frac{V}{2} & \gamma_{\mathbf{k}} \\ 0 & t_z & \gamma_{\mathbf{k}}^\dagger & -\frac{V}{2} \end{pmatrix} \quad (\text{A.7})$$

and hence the eigenenergies will result in

$$\begin{aligned} \varepsilon_1(\xi) &= \pm \frac{1}{2} \sqrt{4t_z^2 + V^2} + \xi \\ \varepsilon_2(\xi) &= \pm \frac{1}{2} \sqrt{4t_z^2 + V^2} - \xi. \end{aligned} \quad (\text{A.8})$$



- [1] C. Berger, Z. Song, T. Li, X. Li, A. Y. Ogbazghi, R. Feng, Z. Dai, A. N. Marchenkov, E. H. Conrad, P. N. First, and W. A. de Heer. Ultrathin Epitaxial Graphite: 2D Electron Gas Properties and a Route Toward Graphene-Based Nanoelectronics. *J. Phys. Chem.*, 108:19912, 2004.
- [2] M. C. Santos Y. G. Pogorelov and V. M. Loktev. Electric Bias Control of Impurity Effects in Bilayer Graphene. *Phys. Rev. B*, 92:075401, 2015.
- [3] K. S. Novoselov, E. McCann, S. V. Morozov, V. I. Fal'ko, M. I. Katsnelson, U. Zeitler, D. Jiang, F. Schedin, and A. K. Geim. Unconventional Quantum Hall Effect and Berry's Phase of  $2\pi$  in Bilayer Graphene. *Nature Physics*, 2:177, 2006.
- [4] G. Fiori and journal = IEEE Electron Device Lett. volume = 30 pages = 1096 year = 2009 G. Iannaccone, title = Ultralow-Voltage Bilayer Graphene Tunnel FET.
- [5] journal = Nature Nanot. volume = 12 pages = 895 year = 2017 M. Kühne, title = Ultrafast Lithium Diffusion in Bilayer Graphene.
- [6] J.-Q. Huang G.-L. Tian J.-Q. Nie H.-J. Peng M.-Q. Zhao, Q. Zhang and journal = Nature Comms. volume = 5 pages = 3410 year = 2014 F. Wei, title = Unstacked Double-Layer Templated Graphene for High-Rate Lithium-Sulphur Batteries.
- [7] H. Yan. Bilayer Graphene: Physics and Application Outlook in Photonics. *Nanophotonics*, 4:115, 2015.
- [8] E. Akbari, R. Yusof, M. T. Ahmadi, A. Enzevae, M. J. Kiani, H. Karimi, and M. Rahmani. Bilayer Graphene Application on NO<sub>2</sub> Sensor Modelling. *J. Nanomat.*, 2014:1, 2014.
- [9] S. V. Morozov D. Jiang M. I. Katsnelson I. V. Grigorieva S. V. Dubonos A. A. Firsov K. S. Novoselov, A. K. Geim. Two-Dimensional Gas of Massless Dirac Fermions in Graphene. *Nature*, 438:197, 2005.
- [10] A. L. Rakhmanov F. Nori A. V. Rozhkov, A. O. Sboychakov. Electronic Properties of Graphene-Based Bilayer Systems. *Phys. Rep.*, 648.
- [11] P. G. Silvestrov and P. Recher. Wigner Crystal Phases in Bilayer Graphene. *Phys. Rev. B*, 95:075438, Feb 2017.
- [12] Gregg Jaeger. The ehrenfest classification of phase transitions: Introduction and evolution. *Archive for History of Exact Sciences*, 53(1):51–81, May 1998.
- [13] E. McCann and M. Koshino. The Electronic Properties of Bilayer Graphene. *Reports on Progress in Physics*, 76(5):056503.
- [14] Zhenhua Qiao, Wang-Kong Tse, Hua Jiang, Yugui Yao, and Qian Niu. Two-Dimensional Topological Insulator State and Topological Phase Transition in Bilayer Graphene. *Phys. Rev. Lett.*, 107:256801, Dec 2011.
- [15] Erez Berg, Mark S. Rudner, and Steven A. Kivelson. Electronic Liquid Crystalline Phases in a Spin-Orbit Coupled Two-Dimensional Electron Gas. *Phys. Rev. B*, 85:035116, Jan 2012.
- [16] Jeil Jung, Marco Polini, and A. H. MacDonald. Persistent Current States in Bilayer Graphene. *Phys. Rev. B*, 91:155423, Apr 2015.
- [17] J.-C. Charlier, J.-P. Michenaud, and X. Gonze. First-Principles Study of the Electronic Properties of Simple Hexagonal Graphite. *Phys. Rev. B*, 46:4531–4539, Aug 1992.
- [18] Zheng Liu, Kazu Suenaga, Peter J. F. Harris, and Sumio Iijima. Open and Closed Edges of Graphene Layers. *Phys. Rev. Lett.*, 102:015501, Jan 2009.
- [19] A. L. Rakhmanov, A. V. Rozhkov, A. O. Sboychakov, and Franco Nori. Instabilities of the *aa*-Stacked Graphene Bilayer. *Phys. Rev. Lett.*, 109:206801, Nov 2012.
- [20] R. S. Akzyanov, A. O. Sboychakov, A. V. Rozhkov, A. L. Rakhmanov, and Franco Nori. *aa*-Stacked Bilayer Graphene in an Applied Electric Field: Tunable Antiferromagnetism and Coexisting Exciton Order Parameter. *Phys. Rev. B*, 90:155415, Oct 2014.
- [21] G. Kresse and J. Furthmuller. Efficient iterative schemes for ab initio total-energy calculations using a plane-wave basis set. *Phys. Rev. B*, 54:11169, 1996.
- [22] G. Kresse and J. Hafner. *Ab initio* molecular dynamics for liquid metals. *Phys. Rev. B*, 47:R558, 1993.
- [23] G. Kresse and J. Furthmuller. Efficiency of ab-initio total energy calculations for metals and

- semiconductors using a plane-wave basis efficient iterative schemes for ab initio total-energy calculations using a plane-wave basis set. *Compt. Mat. Sci.*, 6:15, 1996.
- [24] J. P. Perdew and Alex Zunger. Self-interaction correction to density-functional approximations for many-electron systems. *Phys. Rev. B*, 23:5048–5079, May 1981.
- [25] G. Kresse and D. Joubert. From ultrasoft pseudopotentials to the projector augmented-wave method. *Phys. Rev. B*, 59:1758–1775, Jan 1999.
- [26] P. E. Blöchl. Projector augmented-wave method. *Phys. Rev. B*, 50:17953–17979, Dec 1994.
- [27] Lianhua He, Fang Liu, Geoffroy Hautier, Micael J. T. Oliveira, Miguel A. L. Marques, Fernando D. Vila, J. J. Rehr, G.-M. Rignanese, and Aihui Zhou. Accuracy of Generalized Gradient Approximation Functionals for Density-Functional Perturbation Theory Calculations. *Phys. Rev. B*, 89:064305, Feb 2014.
- [28] Fabio Favot and Andrea Dal Corso. Phonon Dispersions: Performance of the Generalized Gradient Approximation. *Phys. Rev. B*, 60:11427–11431, Oct 1999.
- [29] E. Lora da Silva, Jonathan M. Skelton, Stephen C. Parker, and Aron Walsh. Phase Stability and Transformations in the Halide Perovskite CsSnI<sub>3</sub>. *Phys. Rev. B*, 91:144107, Apr 2015.
- [30] H. J. Monkhorst and J. D. Pack. Special Points for Brillouin-Zone Integrations. *Phys. Rev. B*, 13:5188, 1976.
- [31] K. Parlinski, Z. Q. Li, and Y. Kawazoe. First-Principles Determination of the Soft Mode in Cubic ZrO<sub>2</sub>. *Phys. Rev. Lett.*, 78:4063, 1997.
- [32] L. Chaput, A. Togo, I. Tanaka, and G. Hug. Phonon-phonon interactions in transition metals. *Phys. Rev. B*, 84:094302, 2001.
- [33] A Togo and I Tanaka. First principles phonon calculations in materials science. *Scr. Mater.*, 108:1, Nov 2015.
- [34] A. Togo, F. Oba, and I. Tanaka. First-principles calculations of the ferroelastic transition between rutile-type and CaCl<sub>2</sub>-type SiO<sub>2</sub> at high pressures. *Phys. Rev. B*, 78:134106, 2008.
- [35] J. M. Skelton, S. C. Parker, A. Togo, I. Tanaka, and A. Walsh. Thermal physics of the lead chalcogenides PbS, PbSe, and PbTe from first principles. *Phys. Rev. B*, 89:205203, 2014.
- [36] P. Y. Yu and M. Cardona. *Fundamentals of Semiconductors: Physics and Materials Properties*. Number pp. 104. 1996.
- [37] M. Gajdoš, K. Hummer, G. Kresse, J. Furthmüller, and F. Bechstedt. Linear Optical Properties in the PAW Methodology. *Phys. Rev. B*, 73:045112, 2006.
- [38] Yuehua Xu, Xiaowei Li, and Jinming Dong. Infrared and Raman Spectra of AA-Stacking Bilayer Graphene. *Nanotechnology*, 21(6):065711.
- [39] M. Hanfland, H. Beister, and K. Syassen. Graphite Under Pressure: Equation of State and First-Order Raman Modes. *Phys. Rev. B*, 39:12598–12603, Jun 1989.
- [40] Jae-Kap Lee, Seung-Cheol Lee, Jae-Pyoung Ahn, Soo-Chul Kim, John I. B. Wilson, and Phillip John. The Growth of AA Graphite on (111) Diamond. *The Journal of Chemical Physics*, 129(23):234709, 2008.
- [41] Eduardo V. Castro, K. S. Novoselov, S. V. Morozov, N. M. R. Peres, J. M. B. Lopes dos Santos, Johan Nilsson, F. Guinea, A. K. Geim, and A. H. Castro Neto. Biased Bilayer Graphene: Semiconductor with a Gap Tunable by the Electric Field Effect. *Phys. Rev. Lett.*, 99:216802, Nov 2007.
- [42] G. Semenoff. Condensed-Matter Simulation of a Three-Dimensional Anomaly. *Phys. Rev. Lett.*, 53:2449, 1984.
- [43] Brian Skinner, B. I. Shklovskii, and M. B. Voloshin. Bound State Energy of a Coulomb Impurity in Gapped Bilayer Graphene. *Phys. Rev. B*, 89:041405, Jan 2014.
- [44] Edward McCann. Asymmetry Gap in the Electronic Band Structure of Bilayer Graphene. *Phys. Rev. B*, 74:161403, Oct 2006.
- [45] M. Mohr, J. Maultzsch, E. Dobardžić, S. Reich, I. Milošević, M. Damnjanović, A. Bosak, M. Krisch, and C. Thomsen. Phonon Dispersion of Graphite by Inelastic X-Ray Scattering. *Phys. Rev. B*, 76:035439, Jul 2007.

- [46] Phonons in Bilayer Graphene. <http://tkea.com.ua/siet/archive/2013-t2/130.pdf>.
- [47] Y. Chen S. Li. Thermal Transport and Anharmonic Phonons in Strained Monolayer Hexagonal Boron Nitride. *Scient. Rep.*, 7.
- [48] S. V. Morozov D. Jiang M. I. Katsnelson I. V. Grigorieva S. V. Dubonos A. A. Firsov K. S. Novoselov, A. K. Geim. A Review on the Flexural Mode of Graphene: Lattice Dynamics, Thermal Conduction, Thermal Expansion, Elasticity and Nanomechanical Resonance. *J. Phys.: Condens. Matter*, 27:083001, 2015.
- [49] Alexandr I. Cocemasov, Denis L. Nika, and Alexander A. Balandin. Phonons in Twisted Bilayer Graphene. *Phys. Rev. B*, 88:035428, Jul 2013.
- [50] E. V. Castro, N .M. R. Peres, J. M. B. Lopes dos Santos, F. Guinea, and A. H. Castro Neto. *Strongly Correlated Systems, Coherence and Entanglement*. World Scientific Publishing Co. Pte. Ltd., 2007.
- [51] J. C. Charlier, X. Gonze, and J. P. Michenaud. First-principles study of the electronic properties of graphite. 43:4579, 1991.